Applied Geochemistry 63 (2015) 248–260

Contents lists available at ScienceDirect

Applied Geochemistry

journal homepage: www.elsevier.com/locate/apgeochem

Carbon sequestration and decreased CO_2 emission caused by terrestrial aquatic photosynthesis: Insights from diel hydrochemical variations in an epikarst spring and two spring-fed ponds in different seasons

R. Yang [a], B. Chen [a], H. Liu [b], Z. Liu [a, *], H. Yan [a]

[a] State Key Laboratory of Environmental Geochemistry, Institute of Geochemistry, Chinese Academy of Sciences, 99 Linchengxi Road, Guiyang 550081, China
[b] Department of Earth Sciences, University of Hong Kong, Pokfulam Road, Hong Kong, China

ARTICLE INFO

Article history:
Received 1 August 2015
Received in revised form
10 September 2015
Accepted 14 September 2015
Available online 15 September 2015

Keywords:
Karst surface waters
Diel hydrochemical variations
Underwater photosynthesis
Carbon sequestration
CO_2 emission
Carbonate weathering

ABSTRACT

Whether carbonate weathering could produce a stable carbon sink depends primarily on the utilization of dissolved inorganic carbon (DIC) by aquatic phototrophs (the so-called Biological Carbon Pump-BCP effect). On this basis, water temperature (T), pH, electrical conductivity (EC) and dissolved oxygen (DO) were synchronously monitored at 15-min resolution for one and two days respectively in January and October 2013 in Maolan Spring and the spring-fed midstream and downstream ponds in Maolan Nature Reserve, China. A thermodynamic model was used to link the continuous data to allow calculation of CO_2 partial pressures (pCO_2) and calcite saturation indexes (SI_C). A floating static chamber was placed on the water surface successively at all sites to quantify CO_2 exchange flux between atmosphere and water so as to evaluate the BCP effect. Results show that, in both winter and autumn, remarkable diel variations of hydrochemical parameters were present in the midstream pond where DO, pH, and SI_C increased in the day and decreased during the night while EC, $[HCO_3^-]$, $[Ca^{2+}]$ and pCO_2 showed inverse changes mainly due to the metabolic processes of the flourishing submerged plants, with photosynthesis dominating in the day and respiration dominating at night. However, hydrochemical parameters in the spring and downstream pond show less change since few submerged plants developed there. It was determined that the BCP effect in the midstream pond was 285 ± 193 t C km^{-2} a^{-1} in winter and 892 ± 300 t C km^{-2} a^{-1} in autumn, indicating a potential significant role of terrestrial aquatic photosynthesis in stabilizing the carbonate weathering-related carbon sink.

1. Introduction

Although freshwater covers only a small fraction of the Earth's surface area, inland freshwater ecosystems (particularly lakes, rivers, and reservoirs) can affect regional carbon balances by storing, oxidizing and transporting terrestrial carbon and thus significantly influencing the terrestrial carbon budget (Cole et al., 2007).

By investigating a large number of lakes worldwide, Cole et al. (1994) found that most of these lakes (approximately 87%) are CO_2-supersaturated with an average CO_2 partial pressure (pCO_2) of about three times the value in the overlying atmosphere, indicating that lakes are sources rather than sinks of atmospheric CO_2. However, in addition to being returned to the atmosphere and delivered to the oceans (Schlesinger and Melack, 1981; Meybeck, 1993; Hope et al., 1994; Duarte and Prairie, 2005), there still exists a large amount of carbon from terrestrial sources that is deposited in aquatic sediments (Dillon and Molot, 1997; Kortelainen et al., 2004; Cole et al., 2007). Moreover, considering the combined action of carbonate dissolution (CO_2 capture) and photosynthetic uptake of dissolved inorganic carbon (DIC) by aquatic phototrophs (carbon sequestration), Liu et al. (2010a) suggested that the sequestrated carbon in terrestrial aquatic ecosystems could be a potentially important atmospheric CO_2 sink, which was previously underestimated (Liu et al., 2011; Liu and Dreybrodt, 2015). In order to accurately assess the global carbon budget, one should clarify whether or not the captured CO_2 by carbonate weathering could form a stable carbon sink. This depends primarily

* Corresponding author.
E-mail address: liuzaihua@vip.gyig.ac.cn (Z. Liu).

http://dx.doi.org/10.1016/j.apgeochem.2015.09.009
0883-2927/

on the efficiency of utilization of DIC by aquatic phototrophs and can be investigated by understanding the spatiotemporal hydrochemical variations in the aquatic ecosystems, especially in karst environments (Liu et al., 2015).

Surface waters in karst terrains are generally rich in DIC and could provide a well-defined natural system to study gas exchange between water and atmosphere, calcite deposition, as well as aquatic photosynthesis and respiration (Spiro and Pentecost, 1991). Previous studies have emphasized particular aspects of geochemistry or biology in these waters (Liu et al., 2006, 2008; Parker et al., 2007; Liu et al., 2010b; De Montety et al., 2011; Jiang et al., 2013; Kurz et al., 2013), but data on the interactions among physical, chemical and biological processes in different seasons are still lacking (Liu et al., 2015). These mutually dependent processes should be discussed together, because consideration of water-rock-gas-organism interaction as a whole is required to understand the spatiotemporal hydrochemical variations in karst waters (Liu et al., 2010a; Liu and Dreybrodt, 2015; Liu et al., 2015).

In view of this, a combination of high-resolution hydrochemical monitoring (at an interval of 15 min) and static floating chamber technique were used to investigate diel hydrochemical variations in typical karst aquatic ecosystems, an epikarst spring and the spring-fed two ponds in Maolan National Reserve, China in different seasons, so as to identify the transformation of DIC to organic carbon and determine the potential carbon sequestration in this system.

2. Study area

Maolan National Reserve (Fig. 1), which is located in Libo county, Guizhou province, SW China, has dense virgin evergreen forests growing on cone karst, and is listed by UNESCO as a world nature heritage site (Libo Karst, one of the three clusters of South China Karst, whc.unesco.org). According to a previous study (Liu et al., 2007), the average annual rainfall in the virgin forest area is about 1750 mm, but is 400 mm lower in the surrounding deforested area. Nearly 80% of precipitation occurs in the monsoon season from April to September. The annual mean air temperature here is about 17 °C, with hot summers (June–August) and cold winters (December–February). The lithology of this site is mainly dolomitic limestone of Lower to Middle Carboniferous age (Jiang et al., 2008; Liu et al., 2007).

The sampled spring "Maolan Spring", which is situated at the base of a cone-karst slope and covered by virgin karst forest, is a Ca–HCO_3-type epikarst spring with flow rate ranging from 0.05 to 3 L s^{-1} (Liu et al., 2007). Full views of the spring and spring-fed two ponds in January (winter month) and October (autumn month) are given in Fig. 2. A large quantity of submerged plants (chiefly *Charophyta*) were developed in the midstream pond, but only few plants occur at the other two sites. The spring and the two ponds were modified by the addition of weirs to control the outflow. The spring weir was built in 2002 for long-term monitoring of water stage and flow calculation (Liu et al., 2007), while the weirs for each pond were built in 2004 by local people for freshwater fish farming, which has been abandoned since 2011.

Based on field measurements, the flow rate of the spring was 0.6 L s^{-1} in January and 0.9 L s^{-1} in October and almost stable during the study periods. The areas of midstream and downstream ponds was 280 m^2 and 1300 m^2, respectively. The depth of the water was shallow (20–30 cm) in the midstream pond, so its volume was much smaller (about 60 m^3) than that of the downstream pond (nearly 1300 m^3). The distance from the spring to the midstream pond is 38 m, and the distance between the midstream and downstream ponds sampling sites is 29 m.

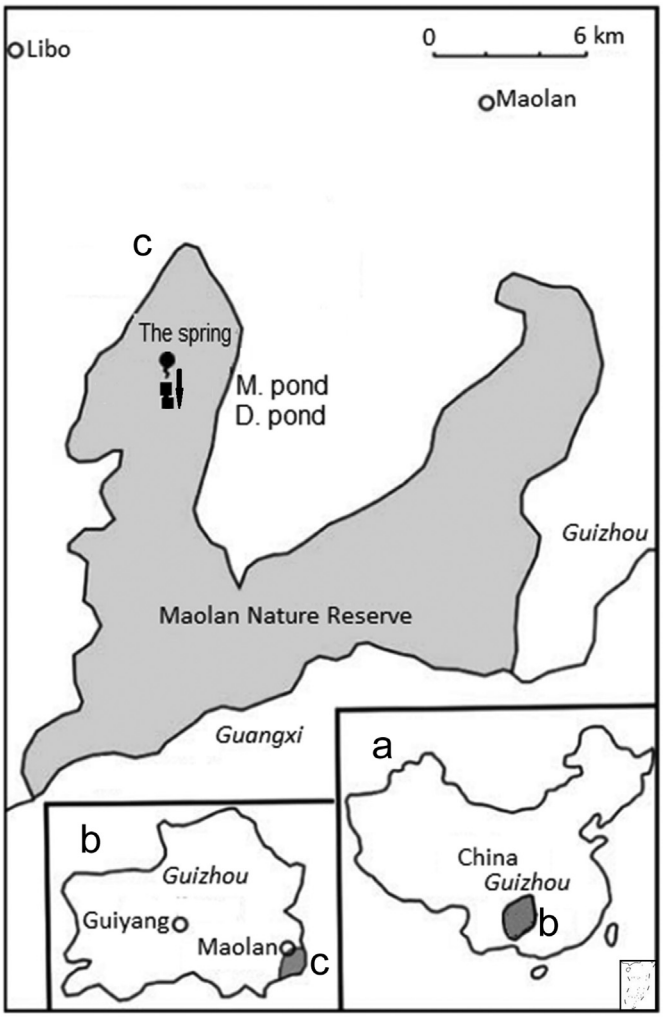

Fig. 1. Geographic location of the field monitoring sites (modified from Jiang et al., (2008)).

3. Methods

3.1. Field automatic monitoring

The field campaigns were conducted under sunny and steady flow conditions on 27–28 January and 24–26 October, 2013 (one diel cycle in winter and two diel cycles in autumn). Three WTW (Wissenschaftlich-Technische-Werkstaetten) Technology Multiline 350i multi-probe were programmed to collect 15-min interval readings of water temperature (T), pH, electrical conductivity (EC, 25 °C), and dissolved oxygen (DO) for the diel cycles. The meters were calibrated prior to deployment using pH (4, 7 and 10), EC (1412 μs cm^{-1}), and DO (0% and 100%) standards. One WTW-350i was placed at the spring orifice to characterize discharging groundwater as much as possible, whereas the other two were operated in the midstream and downstream ponds. The resolutions of pH, T, DO and EC are 0.01, 0.01 °C, 0.01 mg L^{-1} and 0.01 μS cm^{-1}, respectively.

3.2. Sampling and analyzing

A static floating chamber (a cylinder with diameter of 40 cm and volume about 14 L) was placed on the water surface to determine the CO_2 exchange flux between water and air at each site three

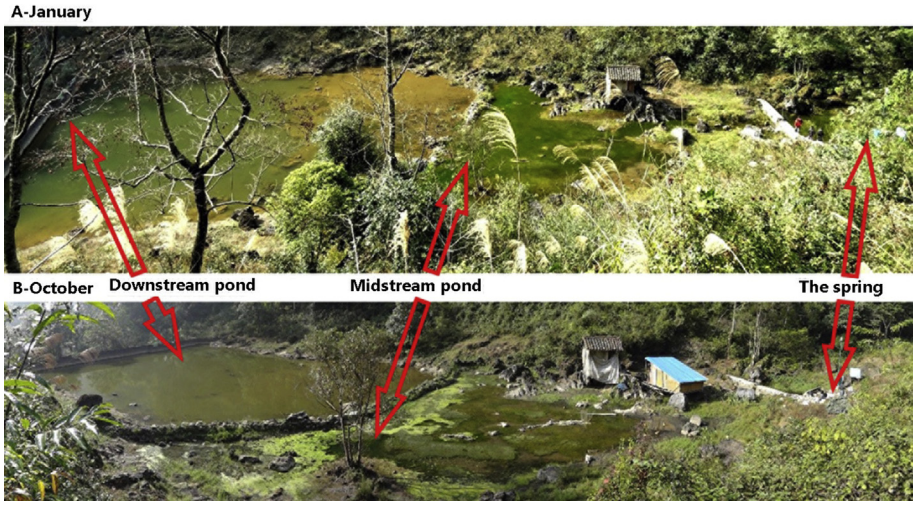

Fig. 2. Full views of Maolan Spring and the spring-fed two ponds in winter (A) and autumn (B). The house (2 m × 2 m × 3 m) beside the midstream pond is for scale.

times a day (early morning, noon and evening). Every 20 mL gas sample was pumped from the chamber by a syringe and injected into a 12-mL vacuum glass vial (sealed by a Teflon cap with rubber plug and pre-vacuumized below 10^{-3} mbar through a vacuum line in the laboratory) at the time of 0, 2, 4, 6, and 8 min. All the gas samples were stored at room temperature and each CO_2 concentration was measured in the laboratory by Agilent-7890 gas chromatography with resolution of 0.01 ppm.

Two sets of water samples were hourly collected through 0.45 μm Millipore filters into 20 ml acid-washed high-density polyethylene bottles for conventional cations and anions analysis. The cations test samples were acidified to pH < 2.0 with concentrated nitric acid to prevent complexation and precipitation. Concentrations of K^+, Na^+ and Mg^{2+} were determined by inductively coupled plasma optical emission spectrometer (ICP-OES) while Cl^-, SO_4^{2-}, NO_3^- and PO_4^{3-} via ICS-90 ion chromatograph. The experimental detecting resolutions of these ions are 0.01 mg L^{-1}. In addition, hourly concentrations of Ca^{2+} and HCO_3^- were in-situ titrated by using Aquamerck hardness test kit and alkalinity test kit, with an estimated accuracy of 1 mg L^{-1} and 0.05 mmol L^{-1} (Liu et al., 2007).

3.3. Estimating CO_2 partial pressure and calcite saturation index

The CO_2 partial pressure (pCO_2) and calcite saturation index (SI_C) were calculated through WATSPEC model (Wigley, 1977) by inputting batch data of pH, T and concentrations of seven major ions. As mentioned earlier, the main lithology in this region is dolomitic limestone, so Ca^{2+} and Mg^{2+} are the major dissolved cations, and HCO_3^- the major counterbalancing anion because of the dissolution of dolomitic limestone. These ions dominate EC in this system. Consequently, continuous concentrations of Ca^{2+}, Mg^{2+} and HCO_3^- can be estimated through the automatically recorded data of EC. According to the hourly in situ titration of $[Ca^{2+}]$ and $[HCO_3^-]$ as well as ion chromatographic analysis of $[Mg^{2+}]$, the linear relationships between concentrations of these ions and EC were established (Fig. 3) as below:

$$\left[Ca^{2+}\right] = 0.20(\pm0.01)EC - 15.44(\pm2.21), \quad R^2 = 0.90,\ P < 0.0001 \tag{1}$$

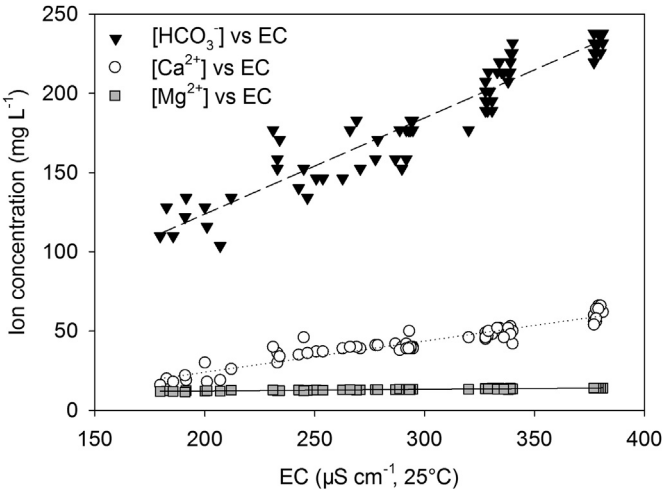

Fig. 3. Linear relationships between $[Ca^{2+}]$, $[Mg^{2+}]$ and $[HCO_3^-]$ versus electrical conductivity (EC).

$$\left[Mg^{2+}\right] = 0.01(\pm0.00)EC + 10.14(\pm0.12), \quad R^2 = 0.91,\ P < 0.0001 \tag{2}$$

$$\left[HCO_3^-\right] = 0.61(\pm0.02)EC + 2.48(\pm6.63), \quad R^2 = 0.91,\ P < 0.0001 \tag{3}$$

The brackets denote species concentrations in mg L^{-1} and EC is electrical conductivity in μS cm^{-1} at 25 °C. It should be noted that EC is a linear relation of the concentrations of all ions in the solution. In fact, only for the pure limestone and dolomite waters (sulfates, nitrates and chlorides (SNC) < 10%) (Krawczyk and Ford, 2006), the concentration of each species (Ca^{2+}, Mg^{2+}, and HCO_3^-) is related to each other due to dissolution of these carbonate minerals.

Data sets of measured T and pH, estimated $[Ca^{2+}]$, $[Mg^{2+}]$, and $[HCO_3^-]$, as well as mean analyzed hourly values of $[K^+]$, $[Na^+]$, $[Cl^-]$ and $[SO_4^{2-}]$ (resolutions are 0.01 mg L^{-1}) were input into WATSPEC program (Wigley, 1977) to calculate pCO_2 and SI_C for each record.

4. Results

Twenty-four hour data of a whole day–night cycle in different seasons (January standing for winter and October for autumn) were summarized in Tables 1 and 2, and presented graphically in Figs. 4–6.

4.1. Diel changes of physicochemical characteristics in the Maolan spring-ponds system

Both in January (winter) and October (autumn), parameters including T, pH, EC, [Ca^{2+}] and [HCO_3^-] in the spring water are almost stable (Figs. 4 and 5) with the variation coefficients (CV) less than 1% except for T, whose CV equal to 1.37 and 1.44, respectively (Table 1). Small changes are found in SI_C, pCO_2 and DO with the CV range from 4.2% to 12.82% (Table 1). Among these parameters, pCO_2 showed lower values during the day and higher values at night, while SI_C and DO showed the opposite (Figs. 4 and 5).

Compared with the spring water, all the physicochemical parameters of the midstream pond water showed marked diel variations in both winter and autumn seasons (Figs. 4 and 5). The CV of T, pH, EC, [Ca^{2+}] and [HCO_3^-] are higher than 4% (compared to below 1% in the spring water), and those of SI_C, pCO_2 and DO are even higher than 44% except for DO in January (CV = 15.93%) (Table 1). Among these parameters, pCO_2 had the highest CV of about 100.35% in January and 112.36% in October. EC, [Ca^{2+}], [HCO_3^-] and pCO_2 decreased during the day and reached the minimum in the late afternoon (about 20:00), then increased during the night and reached the maximum in the early morning (about 08:00), while T, pH, SI_C and DO showed inverse changes (Figs. 4 and 5). In addition, the mean values of pH, SI_C and DO were higher, but EC, [Ca^{2+}], [HCO_3^-] and pCO_2 were lower than those of spring water (Table 1).

In the downstream pond, all of the parameters followed similar patterns of variation to those in the midstream pond and the spring but with CV and mean values similar to the spring (Table 1, Figs. 4 and 5).

4.2. CO_2 efflux and influx in Maolan spring-ponds system

Table 2 and Fig. 6 show the CO_2 fluxes of the spring and spring-fed two ponds. It can be seen that CO_2-degassing is obvious during measuring periods in the spring pool and downstream pond. CO_2-degassing was most intense in the winter evening and the autumn morning for the spring pool (with the highest flux of 37.3 mg m^{-2} h^{-1} and 23.7 mg m^{-2} h^{-1}, respectively); for the downstream pond, CO_2 degassing was most intense in the evening of both winter and autumn (with the highest flux of 21.1 mg m^{-2} h^{-1} and 24.9 mg m^{-2} h^{-1}, respectively). However, for the midstream pond, CO_2-degassing was only observed in the morning, while atmospheric CO_2 was taken into the water at noon and late afternoon during both winter and autumn sampling intervals (negative fluxes in Table 2).

The daily mean fluxes of CO_2 at each site were estimated from the three measured results in the morning, at noon and in the evening and also presented in Table 2. While CO_2 flux variations in the spring and downstream pond are smaller between autumn and winter (0.3-fold and 1.5-fold, respectively), there is apparently more CO_2 sinking into midstream pond in autumn than in winter (4.5-fold).

5. Discussion

5.1. Mechanisms for large diel hydrochemical changes in the midstream pond

Diel physicochemical characteristics of surface waters could be controlled by groundwater input, temperature fluctuations, gas exchange between water and atmosphere, calcite precipitation and dissolution, and aquatic photosynthesis and respiration (Liu et al., 2006, 2008; Spiro and Pentecost, 1991; De Montety et al., 2011; Jiang et al., 2013; Liu et al., 2015).

5.1.1. Groundwater input

According to Table 1, Figs. 4 and 5, little or no diel variations were observed in the physicochemical parameters of the Maolan

Table 1
Statistics on the diel variations of physicochemical parameters in Maolan spring-ponds system in winter month (January) and autumn month (October).

Site name	Spring		Midstream pond		Downstream pond	
Month	January	October	January	October	January	October
T (°C)	15.17–15.87[a] (15.41)[b] [1.37][c]	16.90–17.70 (17.33) [1.44]	10.17–16.57 (13.04) [14.30]	14.10–22.30 (17.78) [15.35]	9.77–13.47 (11.21) [8.39]	16.40–20.40 (18.10) [6.79]
pH	7.97–8.21 (8.09) [0.66]	7.60–7.72 (7.67) [0.36]	7.87–9.12 (8.60) [4.47]	7.91–9.46 (8.72) [5.95]	8.27–8.35 (8.31) [0.23]	8.17–8.46 (8.32) [0.96]
EC(μS cm^{-1})	326.67–330.67 (329.01) [0.35]	377.00–384.00 (379.42) [0.34]	241.67–300.67 (261.53) [6.31]	181.50–337.00 (240.64) [19.69]	287.67–296.67 (292.77) [0.65]	329.00–341.00 (338.06) [0.72]
Ca^{2+}(mg L^{-1})[d]	48.92–49.70 (49.38) [0.46]	58.83–60.21 (59.31) [0.43]	32.17–43.79 (36.08) [9.01]	20.32–50.95 (31.97) [29.20]	41.23–43.01 (42.24) [0.88]	49.38–51.74 (51.16) [0.93]
Mg^{2+}(mg L^{-1})[d]	13.54–13.58 (13.56) [0.09]	14.06–14.13 (14.09) [0.10]	12.65–13.27 (12.86) [1.33]	12.03–13.65 (12.64) [3.90]	13.13–13.23 (13.19) [0.15]	13.56–13.69 (13.66) [0.18]
HCO_3^- (mg L^{-1})[d]	200.77–203.19 (202.19) [0.35]	231.32–235.57 (232.79) [0.34]	149.17–184.98 (161.23) [6.21]	112.65–207.04 (148.55) [19.37]	177.09–182.56 (180.19) [0.64]	202.18–209.47 (207.68) [0.71]
SI_C	0.39–0.62 (0.50) [9.83]	0.19–0.30 (0.26) [9.80]	0.06–1.22 (0.73) [46.47]	0.04–1.37 (0.78) [44.31]	0.50–0.60 (0.55) [4.29]	0.67–0.95 (0.81) [9.79]
pCO_2 (ppmv)	1054–1858 (1427) [12.82]	3890–5176 (4360) [6.80]	89–1914 (517) [100.35]	25–1866 (521) [112.36]	650–780 (724) [4.37]	627–1247 (871) [19.74]
DO (mg L^{-1})	7.78–9.23 (8.31) [4.20]	5.32–8.77 (7.46) [9.54]	8.18–15.27 (11.71) [15.93]	1.89–22.90 (12.30) [53.35]	9.46–10.26 (9.78) [1.97]	3.83–6.70 (5.54) [11.06]

The mean hourly values of the other ions: [K^+] = 0.13 mg L^{-1}, [Na^+] = 0.23 mg L^{-1}, [Cl^-] = 2.03 mg L^{-1}, [SO_4^{2-}] = 11.08 mg L^{-1}, [NO_3^-]: 1.84–5.80 mg/L in January, and 1.42–6.46 mg/L in October. [PO_4^{3-}]: lower than the detection limit in January and ranging from 0.01 to 0.06 mg/L in October.

[a] Minimum–maximum.
[b] Mean values (Number of samples are 96 both in January and October).
[c] CV or variation coefficients = (standard deviation/mean) %.
[d] Calculated values via Equations (1)–(3).

Table 2
Measured CO_2 concentrations in the floating chamber and derived CO_2 flux (F) in Maolan spring-ponds system in winter month (January) and autumn month (October).

Site name		Spring			Midstream pond			Downstream pond	
Month		January	October		January	October		January	October
CO_2 (ppmv)	07:00	413.70	501.26	07:20	404.06	460.76	07:40	401.87	461.85
	07:02	420.88	505.03	07:22	405.80	462.81	07:42	405.10	462.15
	07:04	426.38	508.76	07:24	406.52	466.26	07:44	404.53	463.77
	07:06	428.62	511.23	07:26	408.55	465.66	07:46	405.23	465.23
	07:08	430.11	516.23	07:28	412.34	471.62	07:48	410.61	467.04
F-morning (mg m^{-2} h^{-1})		26.64	23.74		12.68	16.14		11.57	8.84
CO_2 (ppmv)	13:00	407.01	372.46	13:20	390.83	390.75	13:40	389.63	398.63
	13:02	411.02	377.53	13:22	384.32	362.54	13:42	394.36	397.37
	13:04	418.64	377.80	13:24	381.07	352.53	13:44	391.56	402.56
	13:06	418.33	380.66	13:26	379.80	328.76	13:46	395.02	401.02
	13:08	421.06	382.77	13:28	378.14	330.77	13:48	400.20	405.20
F-noon (mg m^{-2} h^{-1})		23.26	15.60		−19.64	−100.99		14.32	11.02
CO_2 (ppmv)	19:00	410.69	421.26	19:20	408.41	405.10	19:40	408.28	453.38
	19:02	410.68	422.60	19:22	407.88	403.25	19:42	413.18	458.18
	19:04	421.90	426.91	19:24	404.44	401.47	19:44	415.01	462.97
	19:06	424.78	424.38	19:26	404.46	400.84	19:46	417.57	466.53
	19:08	432.02	432.67	19:28	400.07	387.59	19:48	422.14	468.14
F-evening (mg m^{-2} h^{-1})		37.28	16.17		−13.21	−24.58		21.08	24.88
F-daily mean (mg $m^{-2}d^{-1}$)		644.82	221.78		−92.84	−419.42		325.89	476.14

$F\ (mg\ m^{-2}\ h^{-1}) = 7.069*(dc/dt)*(V/A)*(273.15/T_m)*(P_m/101.325)$.
$F\ (mg\ m^{-2}d^{-1}) = 169.6*(dc/dt)*(V/A)*(273.15/T_m)*(P_m/101.325)$.
where 7.069 and 169.6: converting factors; dc/dt: change rate of CO_2 concentration in the floating chamber; V: chamber volume (0.014 m^3); A: chamber bottom area (0.1257 m^2); 273.15: standard temperature in K; T_m: the measured temperature of the sampling day in K; P_m: the measured pressure on the sampling day in kPa; 101.325: standard pressure in kPa. The "−" sign indicates CO_2 influx, and the positive values mean effluxes.

Spring. This indicates that groundwater parameters were stable and thus the diel changes in physical and chemical properties in the midstream pond were not caused by changes in the groundwater input.

5.1.2. Temperature fluctuation

Changes in water temperature can affect solubility of minerals and gases on a diel scale (Drysdale et al., 2003). Solubility of both O_2 and CO_2 are temperature-dependent with higher solubility when water temperature is low. On the other hand, changes in temperature can also affect the biological activity (Staehr and Sand-Jensen, 2006): appropriate high temperature can promote the photosynthesis (Davison, 1991), but also accelerate respiration and decomposition of organic matter (Simpson et al., 1980). In this section, we first consider the influence of temperature on solubility. Although pCO_2 variations in the midstream pond follow the temperature-solubility rule, reversed changes in DO were also found (Figs. 4 and 5). It is clear that changes of solubility under different water temperature did not explain the DO fluctuations in the midstream pond. By means of a calculation with the geochemical code PHREEQC (De Montety et al., 2011), the contribution of temperature changes to the daily fluctuations of pCO_2 were estimated to be only 6% in January and October, the remainder of which were probably caused by the temperature-induced biological changes and will be discussed later.

5.1.3. Gas exchange between water and atmosphere

Gas exchange between water and air could induce great diel variations in DO and pCO_2, which controls Eh and pH (Hoffer-French and Herman, 1989; Liu et al., 2006, 2008). Generally, inland streams and rivers tend to be CO_2 supersaturated with respect to atmosphere, and thus are net source of CO_2 to the atmosphere (Butman and Raymond, 2011). However, our results show that there existed both efflux and influx of CO_2 in the midstream pond during study periods (Table 2, Fig. 6). CO_2 degassed in the morning, but was taken into water at noon and in the late afternoon. In this study, pCO_2 and DO followed opposite trends in the midstream pond.

5.1.4. Metabolism of aquatic phototrophs and the calcite precipitation/dissolution

The abovementioned factors all point to an important biological process, the metabolism of aquatic phototrophs, to determine the diel hydrochemical variations in the midstream pond. According to previous studies, diel hydrochemical variations are more commonly influenced by aquatic photosynthesis and respiration processes which could be approximated by the following equations (Liu et al., 2008, 2015):

$$6H_2O + 6CO_2 \xrightarrow{\text{photosynthesis}} C_6H_{12}O_6 + 6O_2 \quad (4)$$

$$C_6H_{12}O_6 + 6O_2 \xrightarrow{\text{respiration}} 6H_2O + 6CO_2 \quad (5)$$

Since O_2 is generated from photosynthesis and consumed through respiration if one ignores O_2 flux through gas exchange, DO, which could reflect O_2 changes in the water, is used as an indicator for discussing the influence of photosynthesis and respiration on diel hydrochemical variations. It was found that, pCO_2 maintained inverse synchronous variations with DO (Figs. 4, 5 and 7) with significant correlations (Table 3), indicating that the metabolism of aquatic phototrophs was the major process controlling the hydrochemical variations in midstream pond during day and night.

During the day, the rate of photosynthesis exceeded that of respiration, CO_2 was consumed and O_2 was accumulated. So, DO and pCO_2 showed inverse direction of change, i.e., DO increased and pCO_2 declined in the water (white arrow in Fig. 7), and thus pH increased (Figs. 4 and 5).

During the night, the rate of respiration and aerobic degradation slowed because of lower water temperature and biological activities. There was no photosynthesis during the night, O_2 in the water was constantly consumed while CO_2 accumulated. Thus, DO decreased, pCO_2 increased (black arrow in Fig. 7), and pH decreased (Figs. 4 and 5) till sunrise at about 8:00.

Temporal variations on calcite saturation usually mirror pH variability, reflecting both the biologically induced seasonal and

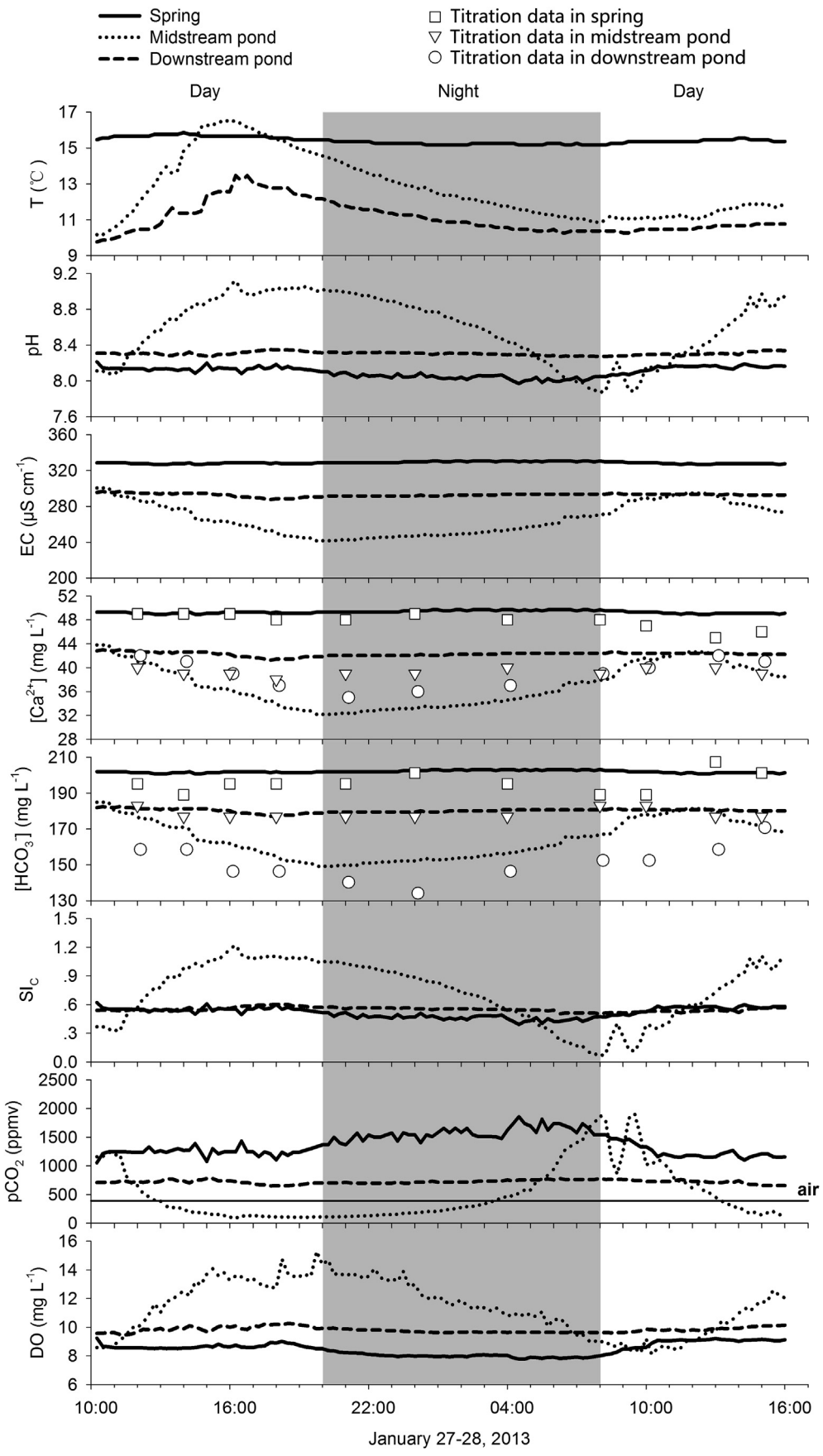

Fig. 4. Diel variations of the physicochemical parameters in Maolan Spring and the spring-fed two ponds through a diel period in winter (January).

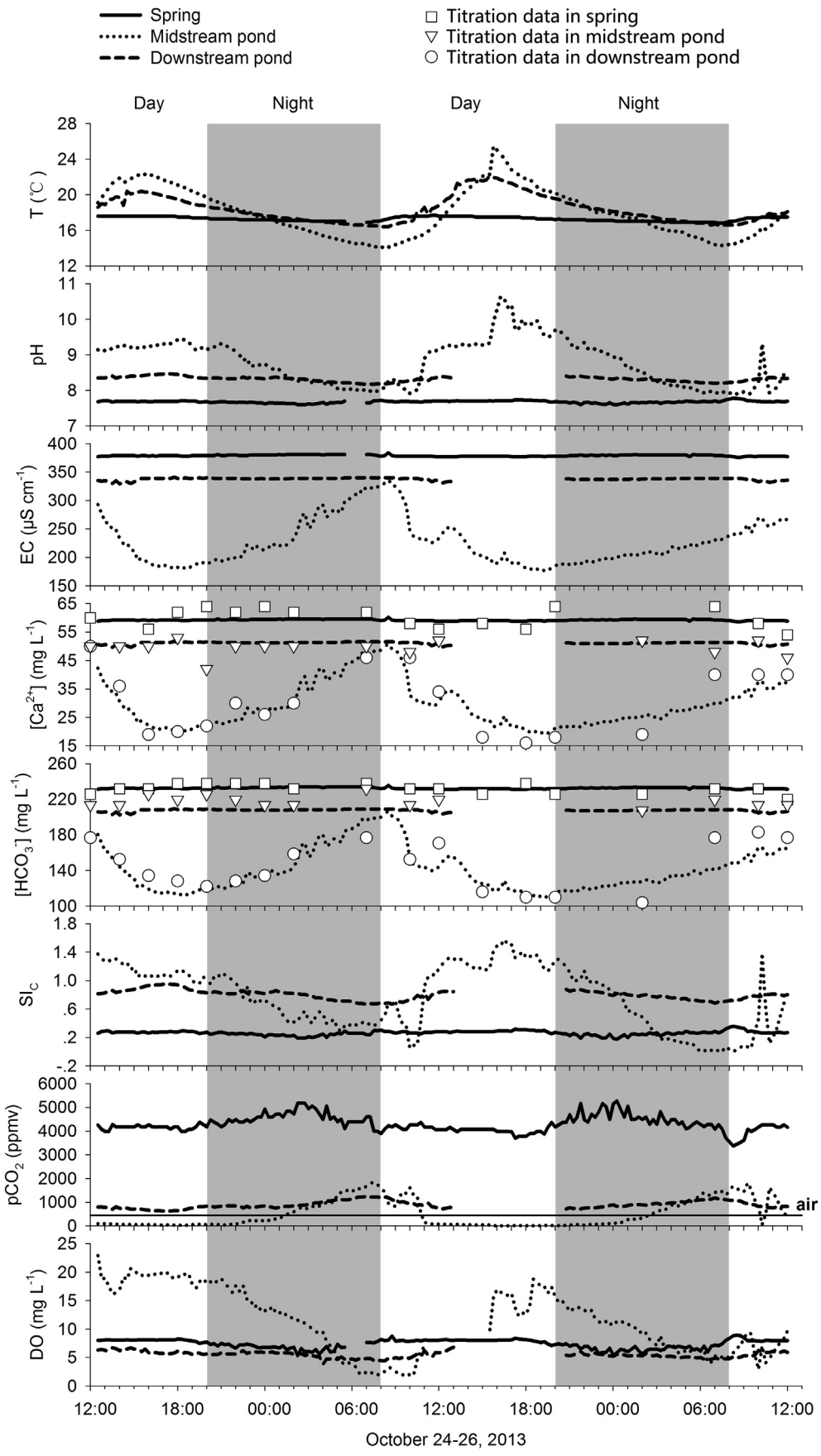

Fig. 5. Diel variations of the physicochemical parameters in Maolan Spring and the spring-fed two ponds through a diel period in autumn (October). The dotted lines on the data sets of downstream pond represent the missing data which were caused by the power outage of WTW MultiLine 350i.

diel changes in dissolved carbon dioxide (Neal et al., 2002). The low pCO_2 as well as high pH and SI_C during the day (Figs. 4 and 5) suggest that submerged plants utilized CO_2/DIC in the water and forced high pH, thereby driving calcite precipitation. At night, with the absence of photosynthesis, CO_2 was continuously released and accumulated through submerged plants respiration and aerobic degradation of organic carbon, hence increasing the solubility of calcite and potentially driving calcite dissolution. These processes can be expressed with the following equations (Liu and Dreybrodt, 2015; Liu et al., 2015):

$$Ca^{2+} + 2HCO_3^- \rightarrow CaCO_3 + x(CO_2 + H_2O) + (1 - x)(CH_2O + O_2), \quad \text{during the day} \tag{6}$$

$$CaCO_3 + CO_2 + H_2O \rightarrow Ca^{2+} + 2HCO_3^-, \quad \text{during night} \tag{7}$$

where x and $1 - x$ are stoichiometric coefficients.

According to Equation (6), calcite precipitation and organic matter formation may decrease EC, $[Ca^{2+}]$ and $[HCO_3^-]$ during the day. But EC, $[Ca^{2+}]$ and $[HCO_3^-]$ may increase owing to calcite dissolution due to release of CO_2 into water from respiration at night. However, recorded SI_C of the midstream water in both seasons ranged from 0.04 to 1.37 (Figs. 4 and 5, Table 1), suggesting calcite was saturated or supersaturated and there was no carbonate dissolution.

5.2. Mechanisms for diel physicochemical variations in the downstream pond

Compared to the midstream pond, diel physicochemical cycles in the downstream pond are similar and can be explained by the factors above. During the day, DO increased but pCO_2 decreased (Figs. 4 and 5) because of preponderant photosynthesis, and thus the pH increased. The inverse variation occurred at night. However, the variation in extent of these parameters in the downstream pond were much less than that in the midstream pond (Table 1). It is likely caused by the larger volume of water in the downstream pond which could buffer the large diel physicochemical variations produced by the midstream pond. The depth of the downstream pond water was around 1–2 m, while the depth of the midstream pond water ranged from 0.2 to 0.6 m. With the surface areas of about 1300 m^2 and 280 m^2, water volumes were estimated to be about 1300 m^3 and 60 m^3 in the downstream and midstream ponds, respectively. Moreover, the large volume effect was further intensified by the much smaller biomass (submerged plants) and accordingly weaker photosynthesis in the downstream pond than in the midstream pond (Liu et al., 2015).

5.3. Differences of physicochemical variations in winter and autumn

Both in January and October, the spring-ponds system showed similar diel physicochemical variations (Figs. 4 and 5) but differences in the mean values of some parameters and the variation amplitude indicated by CV (Tables 1 and 2). Compared with the situation in January (winter), the vegetation biomass and soil temperature were higher in October (autumn), causing stronger root respiration and organic matter decomposition in the soil, thus more CO_2 was generated. Consequently, the spring water in October was characterized by higher pCO_2 and lower pH due to the sensitive response of groundwater geochemistry to soil CO_2 (Yang et al., 2012). On the other hand, higher aquatic biomass and water temperature in the pond systems in October resulted in more intensive photosynthesis (evidenced by higher DO and lower pCO_2 during the day) and respiration (evidenced by lower DO and higher pCO_2 during the night), and thus greater diel change of physicochemical parameters (Table 1).

5.4. Contribution of aquatic biological carbon pump effects to carbon sequestration

5.4.1. Transformation of DIC into organic carbon: carbon stability

The initial DIC in midstream pond was mainly from the spring water and the initial DIC in downstream pond was controlled by the midstream pond water input. DIC concentrations in the midstream and downstream ponds were always lower than those in the spring water (Figs. 4 and 5). The decrease of DIC concentrations between the spring and the two ponds reflects the loss of inorganic carbon in the ponds. The processes influencing the DIC concentrations in the ponds were: (1) calcite precipitation and dissolution, (2) CO_2 exchange with atmosphere, and (3) photosynthetic and respiratory activities.

Since this loss of DIC will be partly transformed into organic carbon, and partly buried eventually as autochthonous organic carbon (Liu and Dreybrodt, 2015), it constitutes a "biological carbon pump" (BCP) (De La Rocha and Passow, 2007; Liu et al., 2010a; Liu and Dreybrodt, 2015; Liu et al., 2015) and increases the carbon stability in the spring-pond system. Moreover, if the terrestrial BCP effect is strong enough, as in the case of the midstream pond, there is even a CO_2 influx from the atmosphere to surface waters (Table 2, Fig. 6), which could directly produce an atmospheric CO_2 sink and will be discussed below in more detail.

5.4.2. CO_2 influx from atmosphere to water: insight from the static floating chamber data in midstream pond

Changes in CO_2 exchange flux between water and atmosphere depend mainly on the pCO_2 variations, which are significantly affected by underwater photosynthesis and respiration, and could be reflected by the changes in DO concentrations. Based on the data of CO_2 flux (Fig. 6, Table 2) and DO (Figs. 4 and 5), a significant relationship between CO_2 flux and DO was found for both winter and autumn (Fig. 8). It showed that when photosynthesis is strong enough, as indicated by DO concentrations > critical values as noted by the vertical dashed lines in Fig. 8, CO_2 in the water was rapidly utilized, resulting in lower pCO_2 than that in atmosphere, and thus a CO_2 influx produced from atmosphere into the water. It is interesting to note that the critical DO concentrations for the change from efflux to influx were different in winter and autumn. They were about 11.3 mg L^{-1} and 9.1 mg L^{-1} for winter and autumn, respectively, which are very close to the equilibrium concentrations of DO with atmospheric O_2 (11.5 mg L^{-1} and 10.1 mg L^{-1}) at the field average water temperature of 12 °C (winter) and 18 °C (autumn) and at the altitude of 600 m at the sampling location (http://www.fivecreeks.org/monitor/do.shtml).

This CO_2 influx suggests that underwater photosynthesis in terrestrial surface waters might produce another important natural carbon sink by taking CO_2 directly from the overlying atmosphere, as happened in the oceans (Ducklow et al., 2001; Passow and Carlson, 2012). Due to the strong BCP effect, the average CO_2 degassing flux for Maolan karst spring-ponds is much less compared with the other karst rivers in the world (Table 4), where underwater photosynthesis may be weak (evidenced by low DO values, generally <8 mg L^{-1} or <100%). When the BCP effect is strong enough, there is even an influx from air to water (Table 4), showing the importance of underwater photosynthesis in both stabilizing the carbon sink (as DIC) by carbonate dissolution and creating new carbon sink directly from overlying atmosphere.

From the fitted regression equation in Fig. 8, one may obtain each CO_2 flux from the corresponding record of DO, and make a quantification of the BCP effect.

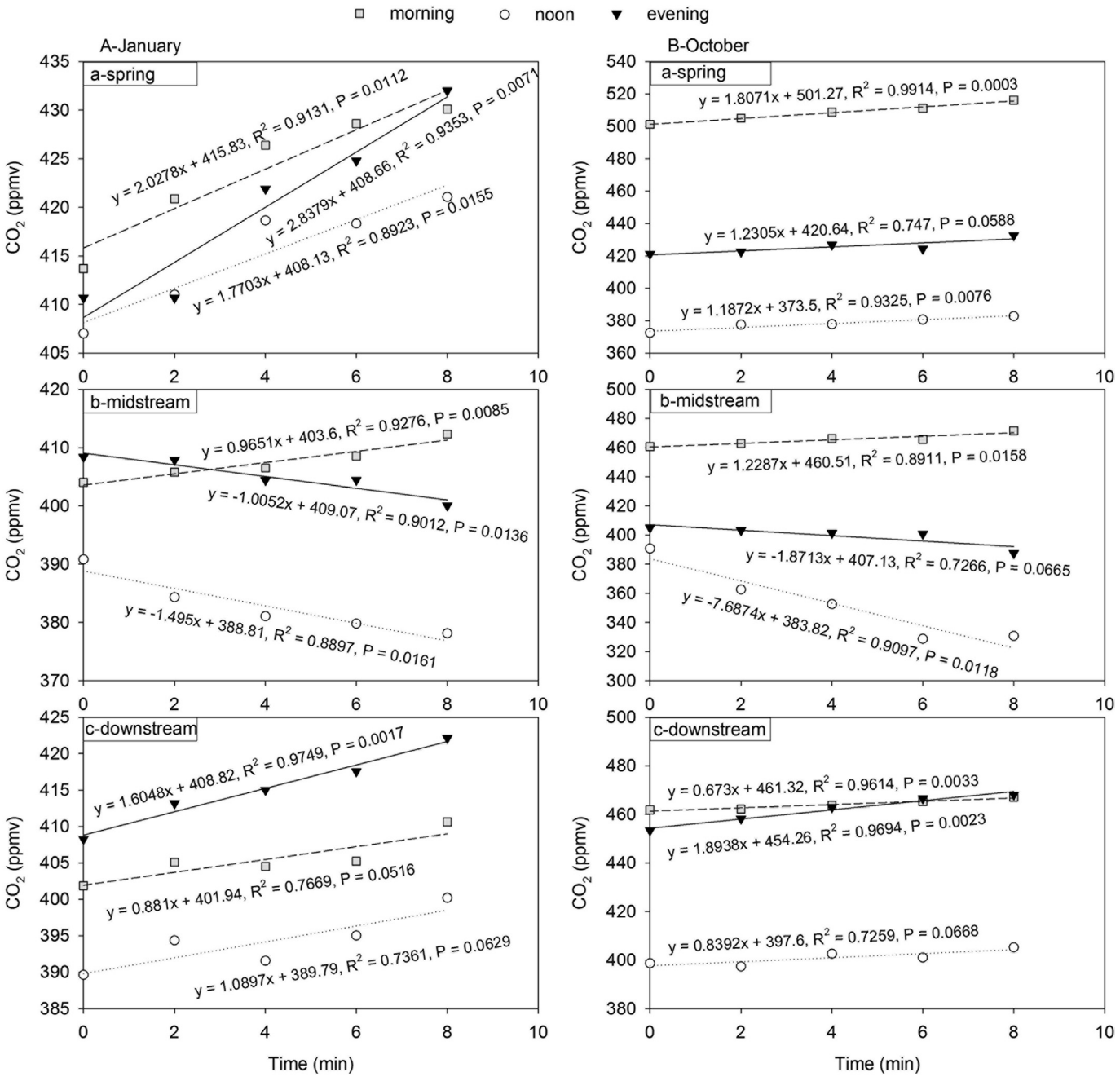

Fig. 6. Temporal variations of CO_2 in the static floating chamber at spring pool (a), midstream pond (b) and downstream pond (c) in winter (A) and autumn (B).

Table 3
Correlations of pCO_2 versus DO in Maolan spring-ponds system in winter month (January) and autumn month (October).

Site name		Spring		Midstream pond		Downstream pond	
Month		January	October	January	October	January	October
pCO_2 vs DO	Pearson Correlation	−0.924[a]	−0.834[a]	−0.883[a]	−0.897[a]	−0.615[a]	−0.829[a]
	Sig. (2-tailed)	0.000	0.000	0.000	0.000	0.000	0.000
	N	96	96	96	96	96	96

[a] Correlation is significant at the 0.01 level (2-tailed).

5.4.3. Quantification of daily organic carbon formation (BCP effect) in the two ponds

The decrease in DIC in the ponds results from the joint effects of calcite precipitation, CO_2 exchange with the atmosphere, and DIC utilization by aquatic photosynthesis (Liu et al., 2015) (Fig. 9). Generally, when pH is 9.6, HCO_3^- and CO_3^{2-} are 84% and 16% of the DIC; when pH is 9, HCO_3^- and CO_3^{2-} constitute 96% and 4% of the DIC. In this study, pH values of the waters at all sites ranged from 7.60 to 9.46. Moreover, only three pH measurements out of a total of 192 for the midstream pond have values higher than 9.4. Thus, the

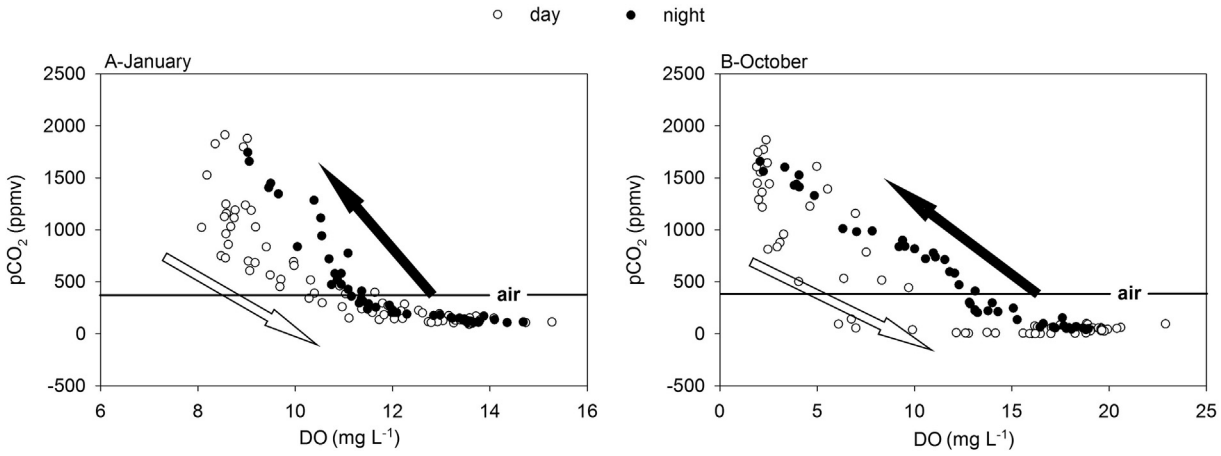

Fig. 7. Correlations between pCO_2 and DO in the midstream pond in winter (A) and autumn (B).

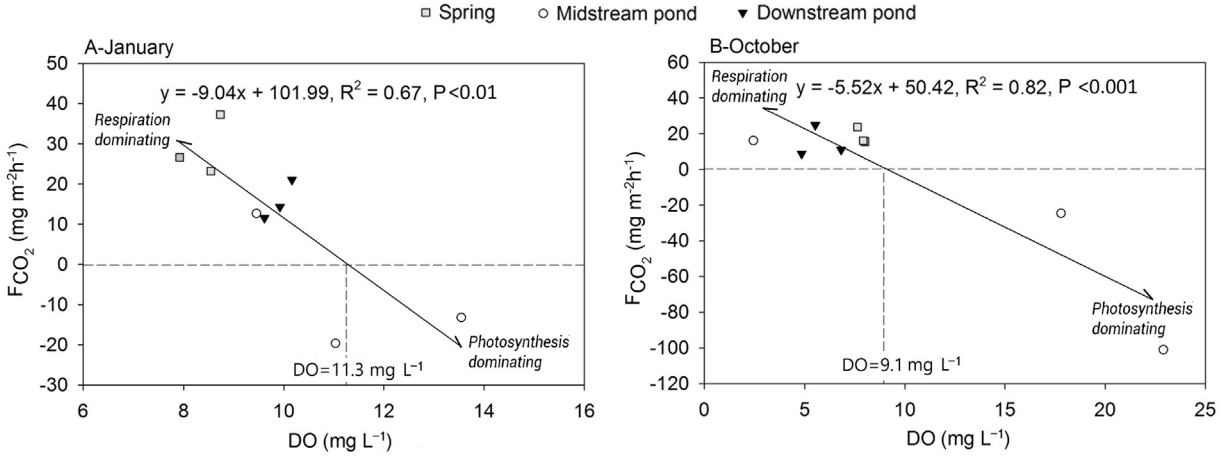

Fig. 8. Measured CO_2 fluxes (F_{CO_2}) versus DO in winter (A) and autumn (B).

Table 4
Comparison of CO_2 degassing to the atmosphere from some carbonate-dominated rivers (streams) in the world.

River	Climate	F_{CO_2} (t C km^{-2} a^{-1})	BCP effect (t C km^{-2} a^{-1})	DO (mg L^{-1})	Ref.
Changjiang river	Subtropic	186–410	NA[a]	72–97%	Zhai et al., 2007
Xijiang river	Humid subtropic	830–1560	NA	NA	Yao et al., 2007
Santa Fe river	Subtropic	402–1156	NA	30–80%	Khadka et al., 2014
Maolan spring-ponds (summer)	Subtropic	−119[b] to 67[c]	677[b] to −49.9[c]	11.31[b]–8.46[c] (8.3 at 28 °C)[d]	Liu et al., 2015
Maolan spring-ponds (autumn)	Subtropic	−42 to 47	892 ± 300 to −176 ± 62	12.3–5.54 (10.1 at 18 °C)	This study
Maolan spring-ponds (winter)	Subtropic	−9 to 32	285 ± 193 to −60 ± 40	11.71–9.78 (11.5 at 12 °C)	This study

[a] Not available; [b] and [c] are the paired values with strong and weak BCP effects respectively; [d] Theoretical value of DO equilibrated with atmospheric O_2 at elevation of 600 m at the sampling site (http://www.fivecreeks.org/monitor/do.shtml).

calculated HCO_3^- (Table 1) is used as an approximation of DIC for this study. In addition, we used the decrease in $[Ca^{2+}]$ (Table 1) to predict calcite precipitation, and the fluxes of CO_2 (Table 2) in the midstream and downstream ponds to estimate the CO_2 exchange with the atmosphere. The daily organic carbon formation in the two ponds can then be estimated as follows:

$$M_{OC} = \int \left(\frac{[DIC]_{in} - [DIC]_{out}}{5.08}\right)_t Qdt - \int \left(\frac{[Ca]_{in} - [Ca]_{out}}{3.337}\right)_t Qdt - \int \left(\frac{F}{3.664}\right)_t Adt \quad (8)$$

where M_{OC} is the mass of organic carbon formed in a day (mg d^{-1}), Q is the flow rate of the stream (i.e., the discharge of the spring if evaporation is ignored under conditions of high humidity in the virgin forests, L s^{-1}), $[DIC]_{in}$ and $[DIC]_{out}$ are the HCO_3^- concentrations (mg L^{-1}) at the inlet and outlet of the ponds, 5.08 is the converting factor between the molar mass of HCO_3^- and carbon, $[Ca]_{in}$ and $[Ca]_{out}$ are the Ca^{2+} concentrations (mg L^{-1}) at the inlet and outlet of the ponds respectively, 3.337 is the converting factor between the molar mass of calcium and carbon, F is the CO_2 flux from water surface (mg m^{-2} s^{-1}), 3.664 is the converting factor between the molar mass of CO_2 and carbon, and A is the area of pond water surface (m^2). The first term denotes the total carbon loss/gain in a pond in a day; the second term is the amount of

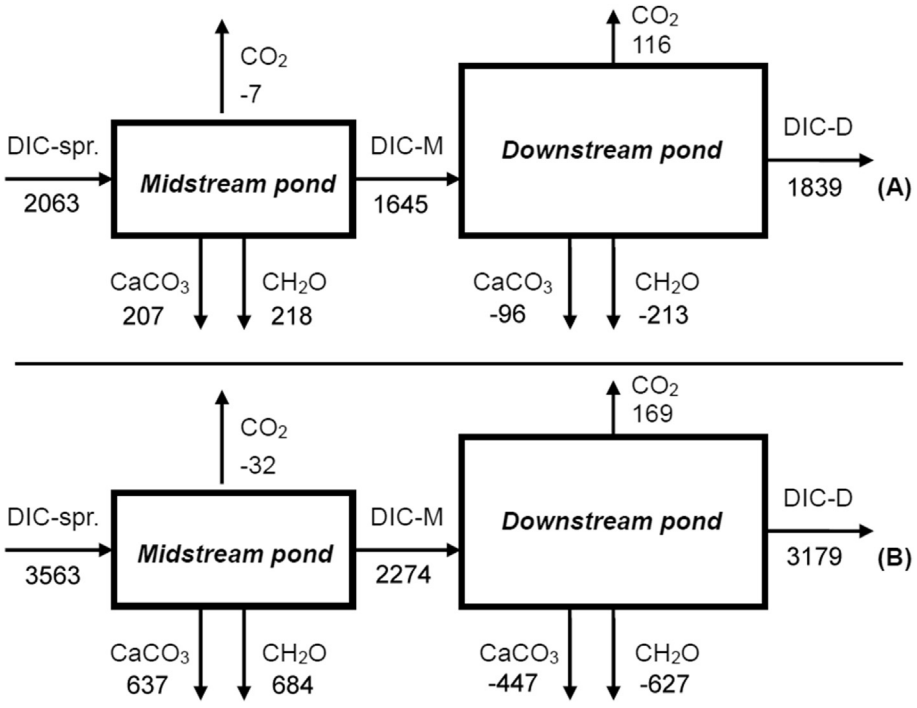

Fig. 9. Daily transport, transfer and mass balance of carbon (g ds^{-1}) in Maolan spring-pond systems in winter (A) and autumn (B), respectively. Note: the box model did not consider the influence of groundwater TOC, which is lower than 5% groundwater DIC. DIC-spr., DIC-M and DIC-D are daily export of DIC (HCO_3^-) from the spring, the midstream and downstream ponds, respectively. Positive values of CO_2, $CaCO_3$ and CH_2O mean CO_2 degassing, calcite precipitation and formation of organic matter in the pond systems, while negative values indicate CO_2 uptake, calcite dissolution and decomposition of organic matter, respectively.

carbon deposited as calcite in a pond in a day; and the third term is the carbon loss/gain via CO_2 exchange in a pond in a day. In this study, dt is 15 min (the interval of automatic recording).

Therefore, the organic carbon sinks formed by submerged plants in the midstream pond are calculated to be 218 ± 148 g d^{-1} in January and 684 ± 230 g d^{-1} in October (Fig. 9), corresponding to the fluxes of 285 ± 193 t C km^{-2} a^{-1} and 892 ± 300 t C km^{-2} a^{-1}, respectively, which are about 43 and 135 times higher than the marine BCP effect (Ducklow et al., 2001), indicating a potential significant role of terrestrial aquatic photosynthesis in stabilizing the carbon sink by carbonate weathering (transformation from DIC to organic carbon, see Equation (6)) and/or uptake of CO_2 directly from the overlying atmosphere. The calculated percentages of transformation from DIC to organic carbon are 52.2% and 53.1%, while 49.5% and 49.4% for the percentages of transformation from DIC to calcite deposits for winter and autumn respectively (Fig. 9). All these indicate the dominating role of terrestrial aquatic photosynthesis in stabilizing the carbon sink by carbonate weathering (HCO_3^- to organic carbon).

The organic carbon sinks in the downstream pond are determined to be −213 ± 144 g d^{-1} in January and −627 ± 221 g d^{-1} in October (Fig. 9), corresponding to the fluxes of −60 ± 40 t C km^{-2} a^{-1} and −176 ± 62 t C km^{-2} a^{-1}. The negative values suggest that there is no net organic carbon sink due to few submerged plants in downstream pond, but a net carbon source to the atmosphere through the decomposition of allochthonous organic matter. We assume this organic matter is the legacy of fish farming, ceased in 2011, in the downstream pond.

Compared with the organic carbon fluxes in winter (January), those in autumn (October) are about 3 times higher for both the midstream and downstream ponds. The large differences may be related to the joint action of the following factors, including light intensity, temperature, and DIC concentration, which control the BCP effects. In general, increase in light intensity and temperature promote the photosynthesis, while rising temperature also increases respiration (Staehr and Sand-Jensen, 2006). The increase in DIC concentration may accelerate the growth of algae, reflecting the DIC fertilization effect (Liu et al., 2010b; Suárez-Álvarez et al., 2012). Due to stronger light intensity, higher water temperature, higher spring DIC concentration (originating from higher content of soil CO_2) (Liu et al., 2007) in autumn, the organic carbon fluxes are higher than those in winter, as happened in the midstream pond. For the downstream pond, higher water temperature in autumn may be the main reason for faster decomposition of allochthonous organic matter, and thus more negative organic fluxes than in the winter.

Curiously, there are both higher positive and negative BCP effects (fluxes) in the autumn study period than those in summer (1.3-fold and 3.5-fold, respectively; Table 4) possibly due to higher underwater light intensity caused by lower turbidity in autumn (with less rainfall and lower discharge, thus lower soil erosion) than in summer (with more precipitation and higher discharge, thus higher soil erosion). However, separate quantification of the contribution by these environmental factors will require future controllable studies.

5.4.4. The fate of sequestered carbon in the midstream pond

The fixed organic carbon in the midstream pond went into two parts: one as TOC transported downstream, and the other as organic matter deposited in the pond. We found that there was an increase in the TOC concentration between the spring and the outlet of midstream pond, from ~2 mg L^{-1} to ~7 mg L^{-1}. In addition, the organic-rich sediment (ooze) accumulation rate was high in the midstream pond. According to field survey, there was about 20 cm of ooze in the pond, which was formed in about 10 years since 2004 when the pond was built by local people. However, the accurate sedimentation and preservation rates of thus-formed autochthonous organic carbon in the pond need to be determined in future

though the soil loss here in the virgin karst forest was low.

6. Conclusions

Physicochemical parameters (T, pH, EC, and DO) were monitored at high time-resolution (15 min) over diel cycles in winter and autumn months to investigate the role of terrestrial aquatic photosynthesis (or BCP effect) in stabilizing the carbonate weathering-related carbon sink and/or uptake of CO_2 directly from the overlying atmosphere at the Maolan Karst Experimental Site, Guizhou province, China. The study site included a karst spring and two downstream ponds with different development of submerged plants, and sampling occurred under sunny, base-flow conditions, when underwater photosynthesis was strong. [Ca^{2+}], [HCO_3^-], pCO_2 and SI_C were estimated from the high-resolution measurements. A floating static chamber was placed on the water surface successively at all sites three times a day (early morning, noon and evening) to quantify CO_2 exchange flux between atmosphere and water.

Results show that, in both winter and autumn seasons, remarkable diel variations of hydrochemical parameters were present in the midstream pond where DO, pH, and SI_C increased during the day and decreased during the night while EC, [HCO_3^-], [Ca^{2+}] and pCO_2 showed inverse changes mainly due to the metabolic process of the flourishing submerged plants (dominated by *Charophyta*) with underwater photosynthesis dominating during the day and respiration dominating during the night. However, hydrochemical parameters in the spring pool and downstream pond show much less change since few submerged plants developed there. Moreover, it was determined that the BCP effect in the midstream pond was 285 ± 193 t C km^{-2} a^{-1} in winter and 892 ± 300 t C km^{-2} a^{-1} in autumn, indicating a potential significant role of terrestrial aquatic photosynthesis in stabilizing the carbonate weathering-related carbon sink (from DIC to organic carbon) and/or uptake of CO_2 directly from the overlying atmosphere.

However, the distribution and extent of surface waters with such a strong BCP is as yet unknown. In addition, sedimentation and preservation rates of thus-formed autochthonous organic carbon in terrestrial surface waters are also poorly known, especially under rapid global climate and land use changes occurring recently. This study suggests that an important goal in improving global carbon budgets may include quantifying the importance of the BCP effect in terrestrial aquatic settings (especially tremendous amount of small streams, ponds, lakes and reservoirs), and thus further research should be taken into account.

Acknowledgments

All data used in this paper can be accessed via email address at rayyangrui@163.com or liuzaihua@vip.gyig.ac.cn. This work was supported by the 973 Project of China (2013CB956703) and the National Natural Science Foundation of China (41430753). Special thanks are given to Ian J. Fairchild (University of Birmingham) for his thoughtful comments and suggestions, which greatly improved the original draft.

References

Butman, D., Raymond, P.A., 2011. Significant efflux of carbon dioxide from streams and rivers in the United States. Nat. Geosci. 4, 839–842.
Cole, J.J., Caraco, N.F., Kling, G.W., Kratz, T.K., 1994. Carbon dioxide supersaturation in the surface waters of lakes. Science 265, 1568–1570.
Cole, J.J., Prairie, Y.T., Caraco, N.F., McDowell, W.H., Tranvik, L.J., Striegl, R.G., Duarte, C.M., Kortelainen, P., Downing, J.A., Middelburg, J.J., Melack, J., 2007. Plumbing the global carbon cycle: integrating inland waters into the terrestrial carbon budget. Ecosystems 10, 172–185.
Davison, I.R., 1991. Environmental effects on algal photosynthesis: temperature. J. Phycol. 27, 2–8.
De La Rocha, C., Passow, U., 2007. Factors influencing the sinking of POC and the efficiency of the biological carbon pump. Deep-sea Res. Pt. II 54, 639–658.
De Montety, V., Martin, J.B., Cohen, M.J., Foster, C., Kurz, M.J., 2011. Influence of diel biogeochemical cycles on carbonate equilibrium in a karst river. Chem. Geol. 283, 31–43.
Dillon, P., Molot, L., 1997. Dissolved organic and inorganic carbon mass balances in central Ontario lakes. Biogeochemistry 36, 29–42.
Drysdale, R., Lucas, S., Carthew, K., 2003. The influence of diurnal temperatures on the hydrochemistry of a tufa-depositing stream. Hydrol. Process 17, 3421–3441.
Duarte, C., Prairie, Y., 2005. Prevalence of heterotrophy and atmospheric CO_2 emissions from aquatic ecosystems. Ecosystems 8, 862–870.
Ducklow, H.W., Steinberg, D.K., Buesseler, K.O., 2001. Upper ocean carbon export and the biological pump. Oceanography 14, 50–58.
Hoffer-French, K.J., Herman, J.S., 1989. Evaluation of hydrological and biological influences on CO_2 fluxes from a karst stream. J. Hydrol. 108, 189–212.
Hope, D., Billett, M.F., Cresser, M.S., 1994. A review of the export of carbon in river water: fluxes and processes. Environ. Pollut. 84, 301–324.
Jiang, G., Guo, F., Wu, J., Li, H., Sun, H., 2008. The threshold value of epikarst runoff in forest karst mountain area. Environ. Geol. 55, 87–93.
Jiang, Y., Hu, Y., Schirmer, M., 2013. Biogeochemical controls on daily cycling of hydrochemistry and $\delta^{13}C$ of dissolved inorganic carbon in a karst spring-fed pool. J. Hydrol. 478, 157–168.
Khadka, M.B., Martin, J.B., Jin, J., 2014. Transport of dissolved carbon and CO_2 degassing from a river system in a mixed silicate and carbonate catchment. J. Hydrol. 513, 391–402.
Kortelainen, P., Pajunen, H., Rantakari, M., Saarnisto, M., 2004. A large carbon pool and small sink in boreal Holocene lake sediments. Glob. Change Biol. 10, 1648–1653.
Krawczyk, W.E., Ford, D.C., 2006. Correlating specific conductivity with total hardness in limestone and dolomite karst waters. Earth Surf. Proc. Landforms 31, 221–234.
Kurz, M.J., de Montety, V., Martin, J.B., Cohen, M.J., Foster, C.R., 2013. Controls on diel metal cycles in a biologically productive carbonate-dominated river. Chem. Geol. 358, 61–74.
Liu, H., Liu, Z., Macpherson, G.L., Yang, R., Chen, B., Sun, H., 2015. Diurnal hydrochemical variations in a karst spring and two ponds, Maolan Karst experimental Site, China: biological pump effects. J. Hydrol. 522, 407–417.
Liu, Y., Liu, Z., Zhang, J., He, Y., Sun, H., 2010b. Experimental study on the utilization of DIC by *Oocystis solitaria* Wittr and its influence on the precipitation of calcium carbonate in karst and non-karst waters. Carb. Evaporites 25, 21–26.
Liu, Z., Dreybrodt, W., 2015. Significance of the carbon sink produced by H_2O-carbonate-CO_2–aquatic phototroph interaction on land. Sci. Bull. 60, 182–191.
Liu, Z., Dreybrodt, W., Liu, H., 2011. Atmospheric CO_2 sink: silicate weathering or carbonate weathering? Appl. Geochem. 26, S292–S294.
Liu, Z., Dreybrodt, W., Wang, H., 2010a. A new direction in effective accounting for the atmospheric CO_2 budget: considering the combined action of carbonate dissolution, the global water cycle and photosynthetic uptake of DIC by aquatic organisms. Earth-Sci. Rev. 99, 162–172.
Liu, Z., Li, Q., Sun, H., Liao, C., Li, H., Wang, J., Wu, K., 2006. Diurnal variations of hydrochemistry in a travertine-depositing stream at Baishuitai, Yunnan, SW China. Aquat. Geochem. 12, 103–121.
Liu, Z., Li, Q., Sun, H., Wang, J., 2007. Seasonal, diurnal and storm-scale hydrochemical variations of typical epikarst springs in subtropical karst areas of SW China: soil CO_2 and dilution effects. J. Hydrol. 337, 207–223.
Liu, Z., Liu, X., Liao, C., 2008. Daytime deposition and nighttime dissolution of calcium carbonate controlled by submerged plants in a karst spring-fed pool: insights from high time-resolution monitoring of physico-chemistry of water. Environ. Geol. 55, 1159–1168.
Meybeck, M., 1993. Riverine transport of atmospheric carbon: sources, global typology and budget. Water Air Soil Poll. 70, 443–463.
Neal, C., Watts, C., Williams, R.J., Neal, M., Hill, L., Wickham, H., 2002. Diurnal and longer term patterns in carbon dioxide and calcite saturation for the River Kennet, south-eastern England. Sci. Total Environ. 282, 205–231.
Parker, S.R., Gammons, C.H., Poulson, S.R., DeGrandpre, M.D., 2007. Diel variations in stream chemistry and isotopic composition of dissolved inorganic carbon, upper Clark Fork River, Montana, USA. Appl. Geochem 22, 1329–1343.
Passow, U., Carlson, C.A., 2012. The biological pump in a high CO_2 world. Mar. Ecol. Prog. Ser. 470, 249–271.
Schlesinger, W.H., Melack, J.M., 1981. Transport of organic carbon in the world's rivers. Tellus 33, 172–187.
Simpson, P.S., Eaton, J.W., Hardwick, K., 1980. The influence of environmental factors on apparent photosynthesis and respiration of the submersed macrophyte Elodea canadensis. Plant Cell Environ. 3, 415–423.
Spiro, B., Pentecost, A., 1991. One day in the life of a stream-a diurnal inorganic carbon mass balance for a travertine-depositing stream (waterfall beck, Yorkshire). Geomicrobiol. J. 9, 1–11.
Staehr, P.A., Sand-Jensen, K.A.J., 2006. Seasonal changes in temperature and nutrient control of photosynthesis, respiration and growth of natural phytoplankton communities. Freshw. Biol. 51, 249–262.
Suárez-Álvarez, S., Gómez-Pinchetti, J., García-Reina, G., 2012. Effects of increased CO_2 levels on growth, photosynthesis, ammonium uptake and cell composition in the macroalga Hypnea spinella (Gigartinales, Rhodophyta). J. Appl. Phycol. 24, 815–823.
Wigley, T.M.L., 1977. WATSPEC: a computer program for determining the

equilibrium speciation of aqueous solutions. Br. Geomorphol. Res. Group Tech. Bull. 20, 1–46.
Yang, R., Liu, Z., Zeng, C., Zhao, M., 2012. Response of epikarst hydrochemical changes to soil CO_2 and weather conditions at Chenqi, Puding, SW China. J. Hydrol. 468, 151–158.
Yao, G., Gao, Q., Wang, Z., Huang, X., He, T., Zhang, Y., Jiao, S., Ding, J., 2007. Dynamics of CO_2 partial pressure and CO_2 outgassing in the lower reaches of the Xijiang River, a subtropical monsoon river in China. Sci. Total Environ. 376, 255–266.
Zhai, W., Dai, M., Guo, X., 2007. Carbonate system and CO_2 degassing fluxes in the inner estuary of Changjiang (Yangtze) River, China. Mar. Chem. 107, 342–356.